Fabrication of Hybrid Nanoparticles with Thermoresponsive Coronas via a Self-Assembling Approach

Yanfeng Zhang,[†] Shizhong Luo,[‡] and Shiyong Liu*[,†,‡]

Department of Polymer Science and Engineering, University of Science and Technology of China, Hefei, Anhui, China, and Laboratory of Macromolecular Colloids and Solutions, The Hefei National Laboratory for Physical Sciences at Microscale, Hefei, Anhui, China

Received August 16, 2005; Revised Manuscript Received September 22, 2005

ABSTRACT: Thermoresponsive polymer-encapsulated silica hybrid nanoparticles were fabricated via self-assembling of block copolymer in aqueous solution into micelles and subsequent sol−gel process inside the micellar core. Poly(*N*-isopropylacrylamide)-*b*-poly(γ-methacryloxypropyltrimethoxysilane) (PNIPAM-*b*-PMPS) was prepared by successive reversible addition−fragmentation transfer (RAFT) polymerizations of *N*-isopropylacrylamide (NIPAM) and γ-methacryloxypropyltrimethoxysilane (MPS) in 1,4-dioxane. In aqueous solution, amphiphilic PNIPAM-*b*-PMPS self-assembles into micelles with PMPS core and PNIPAM shell. Base-catalyzed sol−gel process inside PMPS core results in PNIPAM-encapsulated silica hybrid core−shell nanoparticles. Transmission electron microscopy (TEM), dynamic light scattering (DLS), and static light scattering (SLS) studies reveal monodisperse hybrid nanoparticles with densely grafted PNIPAM brush at the surface of silica core. Grafted PNIPAM brush shows thermoresponsive two-stage collapse upon heating. Because of the high conversion of RAFT polymerization of MPS, we also show that a one-pot synthesis of thermoresponsive hybrid nanoparticles is feasible. This is the first report of stimuli-responsive hybrid core−shell nanoparticles via the block copolymer self-assembling approach.

Introduction

Organic/inorganic hybrid nanomaterials have attracted considerable interests in the past decade due to the fascinating size-dependent optical, magnetic, and electronic properties of particles at the nanoscale.[1−6] Hybrid nanoparticles consist of a polymer with incorporated inorganic nanoparticles; the organic polymer shell determines the chemical properties of nanoparticles, the interaction with the environments, and their responsiveness to external stimuli, while their physical properties are governed by both the size and shape of the inorganic core and the surrounding organic layer.

Hybrid nanoparticles can be prepared by physical adsorption and polymer covalent grafting techniques. The techniques of covalently grafting polymer chains onto nanopaticles can be further categorized into "grafting from"[7−10] and "grafting to".[11−23] Compared to grafting to technique, the "grafting from" technique provides better control over the type of polymer to be grafted onto the particle surface, surface densities, and chain lengths at the nanometer scales. However, the "grafting from" technique usually requires a multistep syntheses of initiator surface-anchored inorganic nanoparticles. The interface between inorganic nanoparticle and polymer shell usually consists of weak covalent bonds (such as ester groups), which is prone to hydrolysis under slightly drastic conditions.

It is well-known that amphiphilic block copolymers can self-assemble into aggregates with various morphologies in water.[23−34] If one block bears reactive functional groups, the morphologies of the aggregates can be fixed by chemical cross-linking.[35−42] This approach can also be used to prepare hybrid core−shell nanoparticles. Starting from a trimethoxysilyl-containing monomer, Chen et al. have synthesized poly(ethylene oxide)-*b*-poly(γ-methacryloxypropyltrimethoxysilane) (PEO-*b*-PMPS) by atom transfer radical polymerization (ATRP); the block copolymer forms vesicles or micelles depending on the relative block length and preparation conditions, etc.[43−46] Gelation of the PMPS block in the self-assembled aggregates successfully fixes their microstructure. It should be noted that the hybrid nanostructures prepared are stabilized by PEO chains, so they are not stimuli-responsive.

MPS is a highly reactive monomer, and it is very sensitive to the presence of water, especially under slightly basic or acid conditions. So every caution must be taken during ATRP polymerization and subsequent purification by column chromatograph to remove the copper catalysts.[44] Reversible addition−fragmentation transfer (RAFT) has recently emerged as a promising controlled radical polymerization technique due to its versatility and simplicity, and the polymer is free from the contamination of metal catalysts. Most importantly, it is compatible with almost all of the conventional free radical polymerization monomers.[47−49] D'agosto has recently reported that RAFT polymerization of MPS can be carried out in a controlled manner; they have also prepared a block copolymer consists of PMPS and poly(methyl methacrylate) (PMMA).[50] Just recently, Benicewicz prepared polystyrene-coated silica nanoparticle via RAFT polymerization using RAFT agent surface-anchored silica nanoparticles.[51]

The applicability of the RAFT technique to MPS monomer indeed opens a door to prepare hybrid nanoparticles with more functionality. Up to now, reports of stimuli-responsive hybrid nanoparticles are still rare;[7−9] most of the literature dealing with stimuli-responsive hybrid nanoparticles uses the "grafting to" technique. This will possibly exert poor control over the grafting density and tedious separation of grafted nanoparticles

[†] University of Science and Technology of China.
[‡] The Hefei National Laboratory for Physical Sciences at Microscale.
* To whom correspondence should be addressed. E-mail: sliu@ustc.edu.cn.

10.1021/ma0518050 CCC: $30.25
Published on Web 10/19/2005

from free polymer chains; most importantly, polymer chains are grafted onto nanoparticles via reversible linkage such as Au−S interactions.[7,8] Herein we present a facile approach to synthesize thermoresponsive polymer-encapsulated silica hybrid nanoparticles via self-assembling of trimethoxysilyl-containing block copolymers and the subsequent sol−gel process. Poly(*N*-isopropylacrylamide)-*b*-poly(γ-methacryloxypropyltrimethoxysilane) (PNIPAM-*b*-PMPS) was prepared by successive reversible addition−fragmentation transfer (RAFT) polymerizations of *N*-isopropylacrylamide (NIPAM) and γ-methacryloxypropyltrimethoxysilane (MPS). In aqueous solution, amphiphilic PNIPAM-*b*-PMPS self-assembles into micelles with PMPS core and PNIPAM shell. The base-catalyzed sol−gel process inside PMPS core results in PNIPAM-encapsulated silica hybrid core−shell nanoparticles. Transmission electron microscopy (TEM), dynamic light scattering (DLS), static light scattering (SLS), and turbidity studies are used to characterize the hybrid core−shell nanoparticles and their thermoresponsiveness. This is believed to be the first preparation of stimuli-responsive hybrid core−shell nanoparticles via the block copolymer self-assembling approach.

Experimental Section

Materials. γ-Methacryloxypropyltrimethoxysilane (MPS) was purchased from Aldrich. It was purified by distillation under reduced pressure. *N*-Isopropylacrylamide (NIPAM) (97%, Tokyo Kasei Kagyo Co.) was purified by recrystallization from a mixture of benzene and *n*-hexane (1/3, v/v). *S*-Benzyl dithiobenzoate (BDTB) was synthesized according to the literature method.[48] 1,4-Dioxane was distilled from $LiAlH_4$. 2,2′-Azobis(isobutyronitrile) (AIBN) was recrystallized from ethanol. Petroleum ether, *n*-hexane, and tetrahydrofuran (THF) were dried by refluxing over sodium and distilled prior to use. *N*,*N*-Dimethylformamide (DMF) was dried over calcium sulfate and distilled at reduced pressure.

RAFT Polymerization of NIPAM. The RAFT polymerization of NIPAM was conducted in a sealed ampule. In a typical run, NIPAM (7.32 g, 64 mmol), BDTB (0.1952 g, 0.8 mmol), and AIBN (32.8 mg, 0.2 mmol) were charged into the glass ampule containing 1,4-dioxane at the molar ratio of 320:4:1. The mixture was degassed through three freeze−thaw cycles. The ampule was then sealed under vacuum and kept in an oil bath at 70 °C to conduct the polymerization. After 24 h, the ampule was put into liquid nitrogen to stop the polymerization. The ampule was broken, and THF was added to dilute the mixture before it was precipitated into 15 times excess of diethyl ether. This precipitation procedure was repeated three times. The resulting slightly pink powder was dried for 12 h under vacuum at room temperature. The molecular weight distribution was determined by gel permeation chromatography (GPC). Linear polystyrene was used as calibration standards. The molecular weight and molecular weight distribution of two PNIPAM homopolymers were determined by GPC using DMF as eluents: $M_n = 12\,100$, $M_w/M_n = 1.08$ and $M_n = 64\,000$, $M_w/M_n = 1.14$, respectively. The degree of polymerization (DP) of the two homopolymers determined by ^{1}H NMR is 48 and 300; they are denoted $PNIPAM_{48}$ and $PNIPAM_{300}$, respectively.

Synthesis of PNIPAM-*b*-PMPS. The polymerization was conducted in a round-bottom flask equipped with a PTFE stopcock with N_2 inlet. A typical polymerization procedure is as follows. The reaction flask was first loaded with $PNIPAM_{48}$ (0.24 g, 4×10^{-5} mol); the polymer was further dried under high vacuum (1×10^{-3} mmHg). Under dry N_2 protection, dry 1,4-dioxane (1.5 mL), freshly distilled MPS (0.4 mL, 1.6×10^{-3} mol), and AIBN (0.0016 g, 1×10^{-5} mol) were loaded. The mixture was degassed through three freeze−thaw cycles. The reaction flask was sealed under vacuum using the PTFE stopcock. It was then kept in an oil bath at 80 °C to conduct the polymerization. After 12 h, the conversion of MPS is higher than 90%, as monitored by ^{1}H NMR. The reaction flask was put into liquid nitrogen to stop the polymerization. Under N_2 protection, dry THF was added to dissolve the viscous mixture; a large amount of dry hexane was added to precipitate the resulting polymer. After decanting the supernatant solution, excess hexane was then added to wash the polymer. Empirically, we found that three cycles of washing−decanting are enough to remove any unreacted MPS monomer. The final product was kept in the reaction flask and dried in a vacuum oven for 12 h at room temperature. Dry N_2 protection is necessary whenever the PTFE stopcock is opened to take out polymer samples. $PNIPAM_{48}$-*b*-$PMPS_{60}$ and $PNIPAM_{300}$-*b*-$PMPS_{52}$ (composition determined by ^{1}H NMR) were synthesized using $PNIPAM_{48}$ and $PNIPAM_{300}$ as macro-RAFT agents, respectively. The molecular weight and molecular weight distribution of $PNIPAM_{48}$-*b*-$PMPS_{60}$ and $PNIPAM_{300}$-*b*-$PMPS_{52}$ are characterized by GPC: $M_n = 24\,000$, $M_w/M_n = 1.10$ and $M_n = 88\,400$, $M_w/M_n = 1.17$, respectively.

General Procedures for Micellization and Sol−Gel Process. Two methods are used to prepare the hybrid micelles. *Method 1*: PNIPAM-*b*-PMPS (50 mg) was dissolved in 5 mL of DMF; under stirring, water was then added dropwise through a syringe at a rate of 1 drop every 5 s. At desired water/DMF ratio, water addition was stopped, and the mixture was left stirring for an additional 12 h. Triethylamine (100 μL) was then added to induce the hydrolysis and polycondensation within the micellar core. After the sol−gel process, DMF was removed by dialysis against deionized water for 3 days. *Method 2*: Another more facile approach to prepare the micelles is conducted by adding 10 mL of 10 g/L PNIPAM-*b*-PMPS solution in DMF quickly into 90 mL of deionized water under vigorous stirring; after 12 h, triethylamine was added. DMF was then removed by dialysis against deionized water.

Characterization. *Nuclear Magnetic Resonance (NMR) Spectroscopy*. All ^{1}H NMR spectra were recorded using a Bruker 300 MHz spectrometer. PNIPAM and PNIPAM-*b*-PMPS samples were analyzed in $CDCl_3$.

Gel Permeation Chromatography (GPC). Molecular weight distributions were determined by GPC using a series of two linear Styragel columns HT3, HT4 and a column temperature of 60 °C. A Waters 1515 pump and a Waters 2414 differential refractive index detector (set at 30 °C) were used. The eluent was DMF + 1 g/L BrLi at a flow rate of 1.0 mL/min.

Laser Light Scattering (LLS). A commercial spectrometer (ALV/DLS/SLS-5022F) equipped with a multitau digital time correlation (ALV5000) and a cylindrical 22 mW UNIPHASE He−Ne laser ($\lambda_0 = 632$ nm) as the light source was used. In static LLS (SLS), we can obtain the weight-average molar mass (M_w) and the *z*-average root-mean-square radius of gyration ($\langle R_g^2\rangle^{1/2}$ or written as $\langle R_g\rangle$) of polymer chains in a dilute solution from the angular dependence of the excess absolute scattering intensity, known as the Rayleigh ratio $R_{vv}(q)$, as

$$\frac{KC}{R_{vv}(q)} \approx \frac{1}{M_w}\left(1 + \frac{1}{3}\langle R_g^2\rangle q^2\right) + 2A_2C \qquad (1)$$

where $K = 4\pi n^2(dn/dC)^2/(N_A\lambda_0^4)$ and $q = (4\pi n/\lambda_0)\sin(\theta/2)$ with N_A, dn/dC, n, and λ_0 being the Avogadro number, the specific refractive index increment, the solvent refractive index, and the wavelength of the laser light in a vacuum, respectively, and A_2 is the second virial coefficient. dn/dC was determined using an Optokem differential refractometer operating at 632.8 nm. Strictly speaking, here $R_{vv}(q)$ should be $R_{vu}(q)$ because there is no analyzer before the detector. However, the depolarized scattering of the solution studied is insignificant so that $R_{vu}(q) \sim R_{vv}(q)$. Also note that in this study the sample solution was so dilute that the extrapolation of $C \rightarrow 0$ was not necessary, and the term $2A_2C$ in eq 1 can be neglected.

In dynamic LLS (DLS), the Laplace inversion of each measured intensity−intensity time correlation function $G^{(2)}(q,t)$ in the self-beating mode can lead to a line-width distribution $G(\Gamma)$. For a pure diffusive relaxation, Γ is related to the

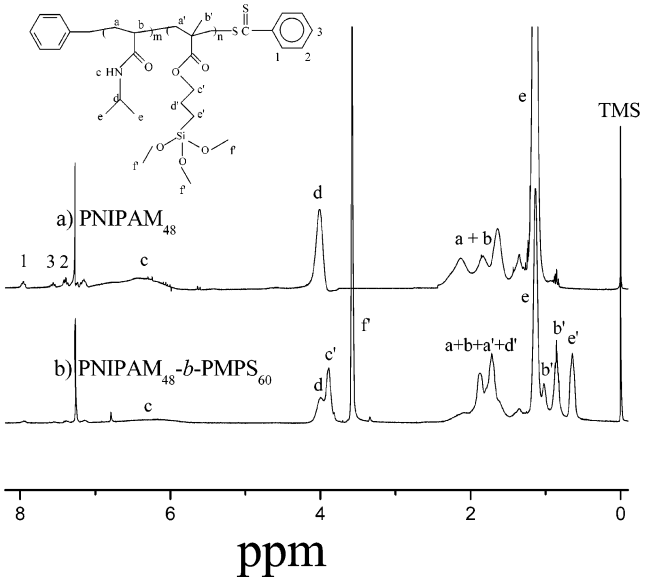

Figure 1. ^{1}H NMR spectra of PNIPAM and PNIPAM-*b*-PMPS in $CDCl_3$.

translational diffusion coefficient D by $(\Gamma/q^2)_{C\to 0,q\to 0} \to D$ or further to the hydrodynamic radius R_h via the Stokes−Einstein equation, $R_h = (k_BT/6\pi\eta_0)/D$, where k_B, T, and η_0 are the Boltzmann constant, the absolute temperature, and the solvent viscosity, respectively.

UV−vis Transmittance Measurements. The transmittance of the solution was measured at a wavelength of 500 nm using a thermostatically controlled cuvette.

Transmission Electron Microscopy (TEM). TEM observations were conducted on a Philips CM 120 electron microscope at an acceleration voltage of 100 kV. The sample for TEM observations was prepared by placing 10 μL of nanoparticle solutions on copper grids coated with thin films of Formvar and carbon successively. No staining was required.

Results and Discussion

Synthesis of PNIPAM-*b*-PMPS. Our initial attempts to synthesize PMPS block first and then use it as a macro-RAFT agent to polymerize NIPAM failed. PMPS is a very viscous solid and very difficult to handle.[50] If PMPS homopolymer was isolated by successive precipitation and dried under high vacuum for more than 3 days, only partial solubility in 1,4-dioxane can be achieved. This indeed brings about complexities for their use as macro-RAFT agent for the polymerization of NIPAM. Fortunately, the target block copolymer can be synthesized by RAFT polymerization of NIPAM block first and then use it as a macro-RAFT agent to polymerize MPS. NIPAM was polymerized using *S*-benzyl dithiobenzoate (BDTB) as the RAFT agent at 60 °C. The ^{1}H NMR spectrum of PNIPAM in $CDCl_3$ shown in Figure 1a reveals the presence of signals characteristic of PNIPAM at $\delta = 5.8-7.0$, 4.0, and 1.2 ppm and the presence of signals at $\delta = 7.9$, 7.6, and 7.4 ppm, which are ascribed to the dithiobenzoyl groups located at the PNIPAM chain end.[52]

Two PNIPAM homopolymers are synthesized, and their molecular weight distributions are characterized by GPC in DMF using polystyrene calibration. Two narrowly distributed PNIPAM homopolymers are obtained: $M_n = 12\,100$, $M_w/M_n = 1.08$ and $M_n = 64\,000$, $M_w/M_n = 1.14$, respectively. A typical molecular weight distribution for the latter homopolymer is shown in Figure 2a. We found that GPC in DMF using PS calibration tends to overestimate the molecular weight

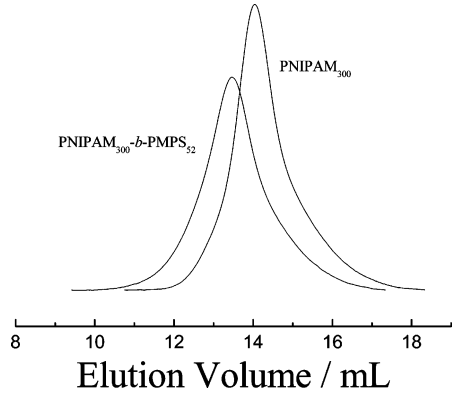

Figure 2. GPC traces of $PNIPAM_{300}$ macro-RAFT agent and $PNIPAM_{300}$-*b*-$PMPS_{52}$.

of PNIPAM. So the actual degrees of polymerization (DP) of two PNIPAM homopolymers were determined by ^{1}H NMR to be 48 and 300; they are denoted $PNIPAM_{48}$ and $PNIPAM_{300}$, respectively.

The PNIPAM homopolymer was then used as a macro-RAFT agent to polymerize MPS. As described in the experimental part, great caution was made to avoid possible gelation of the reaction mixture due to the presence of reactive trimethoxysilyl functions. A gradual increase of viscosity was observed during polymerization. Typical conversion reaches higher than 90% after 12 h. The final product is wholly soluble in THF and 1,4-dioxane; it can be kept in the solid form for months without any appreciable gelation. The ^{1}H NMR spectrum in $CDCl_3$ of the final product (Figure 1b) reveals the presence of signals from both PNIPAM and PMPS block. Characteristic signals from trimethoxysilyl protons at $\delta = 3.60$ appear as a singlet, indicating no hydrolysis or condensation of trimethoxysilyl functions takes place during polymerization and the subsequent purification process. Most importantly, GPC traces in Figure 2 clearly show that the elution peak shift to higher molecular weight after block copolymerization. The diblock copolymer elution peak is relatively symmetric and shows no appreciable tailing at the lower molecular weight side, indicating a complete consumption of PNIPAM macro-RAFT agent. The block copolymer compositions were calculated from the ^{1}H NMR spectrum; $PNIPAM_{48}$-*b*-$PMPS_{60}$ and $PNIPAM_{300}$-*b*-$PMPS_{52}$ are obtained. Molecular weights and their distributions are characterized by GPC analysis in DMF using polystyrene calibration: $M_n = 24\,000$, $M_w/M_n = 1.10$ for $PNIPAM_{48}$-*b*-$PMPS_{60}$ and $M_n = 88\,400$, $M_w/M_n = 1.17$ for $PNIPAM_{300}$-*b*-$PMPS_{52}$. D'agosto et al. have reported that RAFT polymerization of MPS can be carried out in a controlled manner, they also prepared poly(methyl methacrylate)-*b*-poly(γ-methacryloxypropyltrimethoxysilane) (PMMA-*b*-PMPS) using PMMA macro-RAFT agent.[50] Here we did not study in detail the kinetics of RAFT polymerization of MPS monomer using the PNIPAM macro-RAFT agent.

TEM Characterization. PNIPAM homopolymer is soluble in water, while PMPS homopolymer is water-insoluble. So in aqueous solution, PNIPAM-*b*-PMPS block copolymers will self-assemble into micelles with PMPS as the core and PNIPAM as the corona. However, both $NIPAM_{48}$-*b*-$PMPS_{60}$ and $PNIPAM_{300}$-*b*-$PMPS_{52}$ cannot be directly dissolved in water; cosolvents need to be used to facilitate the self-assembly. A typical organic solvent such as methanol or THF cannot be used as cosolvent due to the cononsolvency of THF/water and

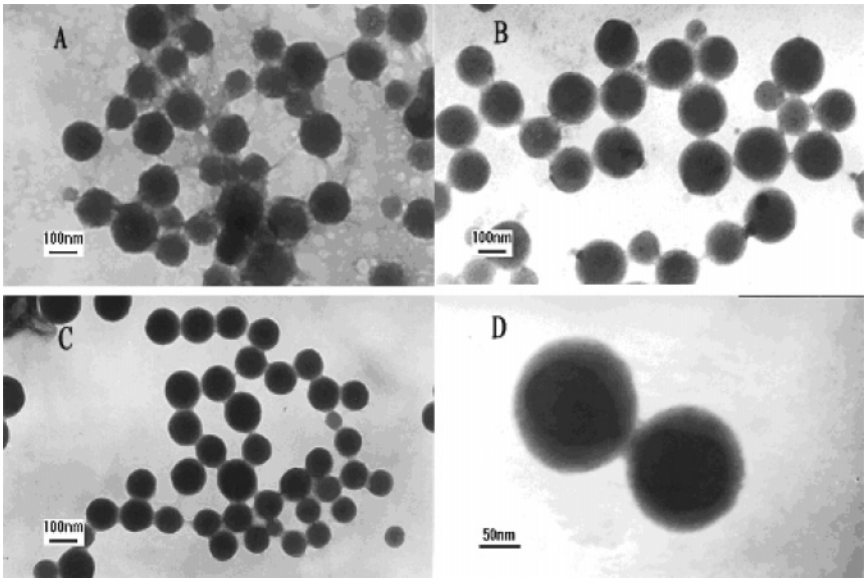

Figure 3. TEM images of the gelated hybrid nanoparticles prepared from $PNIPAM_{48}$-*b*-$PMPS_{60}$ by method 1 at different water contents: A, 15% v/v; B, 30% v/v; C, 50% v/v; D, 50% v/v.

methanol/water to PNIPAM block; i.e., PNIPAM homopolymer is not soluble in THF/water and methanol/water mixture at intermediate volume ratios. Fortunately, PNIPAM is soluble in the DMF/water mixture at any ratio.

Micelles forms spontaneously when water is added into the DMF solution of $PNIPAM_{48}$-*b*-$PMPS_{60}$ at an initial concentration of 1.0×10^{-2} g/mL (method 1). The first few drops of water added water result in no apparent change of the solution, which still keeps clear. At water content higher than 12.2% v/v, a slightly bluish tinge was observed. With continual water addition, the solution turns slightly milky and finally stabilized at water contents higher than 50% v/v. The nanoparticles formed in solution undergo sol−gel processes upon addition of triethylamine, which will chemically cross-link the PMPS core.[43−46] Figure 3 shows typical TEM images of dialyzed nanoparticles prepared at different water contents and after cross-linking. At 15% v/v water content (Figure 3a), robust monodisperse spherical nanoparticles with diameters 130−160 nm coexist with some honeycomb-like network structures, indicating incomplete micellization when the water content is relatively low. At 30% and 50% v/v water content, only spherical nanoparticles are observed. Relatively smaller nanoparticles with diameters 100−120 nm are formed at 50% v/v water content compared to that at 30% v/v water content (130−160 nm in diameter).

Figure 3d shows enlarged hybrid nanoparticles formed at 50% v/v water content. We can clearly observe the core−shell nanostructure; the thickness of the gray shell is about 20−30 nm. PNIPAM blocks with a DP of 48 are not expected to be stretched to this extent. Since the PMPS block shows much better contrast than the PNIPAM block, the observed core−shell structure actually reflects the density distribution of the PMPS block, with the dark core composed of a high density of PMPS and the gray shell composed of much lower density of PMPS. The hybrid nanoparticles in aqueous solution are stabilized by the surrounding soluble PNIPAM chains, which are invisible under TEM observation.

The size of the hybrid nanoparticles prepared by method 1 is very large considering the chemical structure of $PNIPAM_{48}$-*b*-$PMPS_{60}$. If all polymer chains are in a stretched conformation, the diameter of the micelles in solution should not exceed $108 \times 2 \times 0.25$ nm = 54 nm. Thus, some PNIPAM blocks must be located inside the nanoparticles. A closer examination of the observed morphologies reveals that the nanoparticle core appears to be composed of multiple subunits (Figure 3c). We thus tentatively ascribe the formation of large hybrid nanoparticles to large compound micelles (LCM).[53] Loose aggregates form first upon initial water addition; under TEM observation, they appear as honeycomb-like network structures with low contrast, as shown in the background of Figure 3a. Upon further water addition, loose aggregates fuse into the observed large spherical nanoparticles, accompanying with the complete disappearance of loose aggregates (Figure 3b,c).

Preparation of hybrid nanoparticles can also be conducted by quick addition of polymer solution in DMF into water under vigorous stirring (method 2). Figure 4 shows the TEM images of hybrid nanoparticles prepared from $PNIPAM_{48}$-*b*-$PMPS_{60}$ and $PNIPAM_{300}$-*b*-$PMPS_{52}$. Fairly monodisperse, much smaller spherical nanoparticles are observed. The diameters of the spherical nanoparticles are 40−60 and 20−40 nm for $PNIPAM_{48}$-*b*-$PMPS_{60}$ and $PNIPAM_{300}$-*b*-$PMPS_{52}$ block copolymers, respectively. Using method 2, the block copolymer chains undergo drastic changes in solvent conditions, nanoparticles formed from aggregation of hydrophobic PMPS block, which is simultaneously stabilized by the hydrophilic PNIPAM. Although this reflects a kinetic stabilization of the nanoparticles, we will show later that the subsequent sol−gel process inside the micellar core permanently fixed the core−shell structure, and the resulting hybrid core−shell nanoparticles are highly stable. A schematic illustration of the preparation of hybrid core/shell nanoparticles is shown in Scheme 1.

LLS Characterization. It is well-known that PNIPAM homopolymer undergoes a coil-to-globule phase transition in dilute aqueous solution at its LCST of ca. 32 °C. PNIPAM homopolymer is no longer soluble at temperature higher than 32 °C.[54] Dynamic and static LLS were then used to characterize the size and size distribution of the prepared hybrid nanoparticles in solution at different temperatures. Figure 5 shows a typical hydrodynamic radius $\langle R_h \rangle$ distribution of hybrid

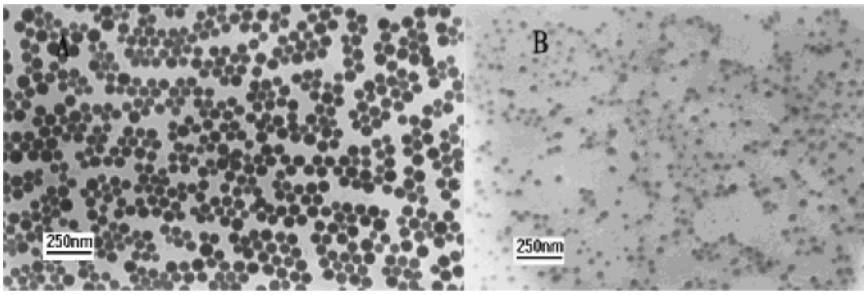

Figure 4. TEM images of the gelated hybrid nanoparticles prepared from (A) $PNIPAM_{48}$-*b*-$PMPS_{60}$ and (B) $PNIPAM_{300}$-*b*-$PMPS_{52}$ by method 2.

Scheme 1. Schematic Illustration of the Preparation of Hybrid Nanoparticles and the Thermoresponsive Collapse of the Shell

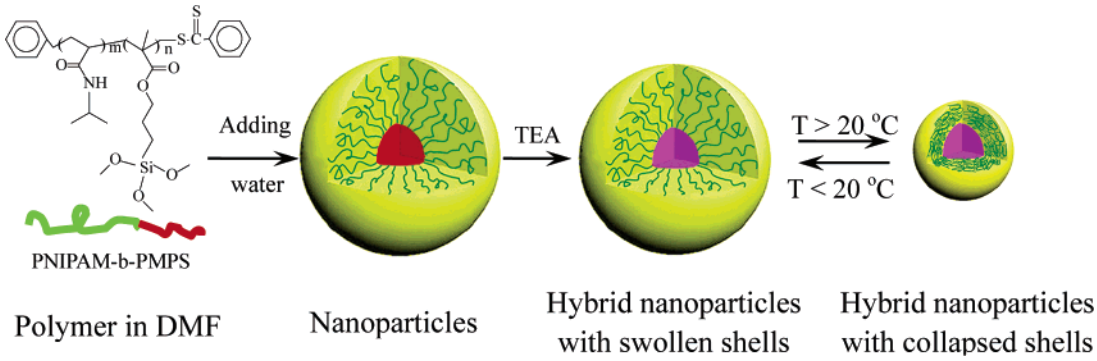

nanoparticles prepared from $PNIPAM_{300}$-*b*-$PMPS_{52}$ by method 2. At 20 °C, R_h of the hybrid nanoparticles ranges from 32 to 114 nm with the peak located at 65 nm. Upon heating the solution to 40 °C, R_h is in the range 25−85 nm with the peak located at 42 nm. This reveals a decrease of particle size upon heating. This must be due to the collapse of PNIPAM brush at the silica core surface. The polydispersity indexes of the size distributions (μ_2/Γ^2) are typically less than 0.08 over the temperature range 20−40 °C, indicating that the nanoparticles are relatively monodisperse; this is also in agreement with the TEM results shown in Figure 4.

It should also be noted that the prepared nanoparticles are very stable. The size and size distribution remain the same after months of storage at low temperature (<30 °C) or upon dilution (more than 1000 times). For nanoparticle concentrations higher than 0.5 g/L, slightly heating to above 35 °C will turn the solution from bluish to turbid. Visually this is a reversible process, since cooling the solution to below 25 °C will reverse it back to the original dispersion with a bluish tinge.

Figure 6 shows the temperature dependence of apparent molecular weight ($M_{w,app}$) of the nanoparticles prepared from $PNIPAM_{300}$-*b*-$PMPS_{52}$ by method 2. The d*n*/d*C* of the nanoparticle solution was determined to be 0.178 mL/g at 20 °C, which is comparable to that of PNIPAM homopolymer in water. The same d*n*/d*C* value was used at all temperatures, assuming that the temperature effect on the d*n*/d*C* is negligible. $M_{w,app}$ keeps almost constant over the temperature range 20−40 °C. This indicates that at a low concentration of 5.0×10^{-6} g/mL used for LLS there is no aggregation between hybrid nanoparticles. PNIPAM chains in the brush only collapse and aggregate within each core−shell nanoparticle. The apparent molecular weight of the nanoparticles is 2.15×10^7 g mol^{-1}. During hydrolysis and cross-linking, three $-O_{1/2}CH_3$ groups will be lost from one MPS monomer unit if we assume that hydrolysis and cross-linking is 100% complete. The number-aver-

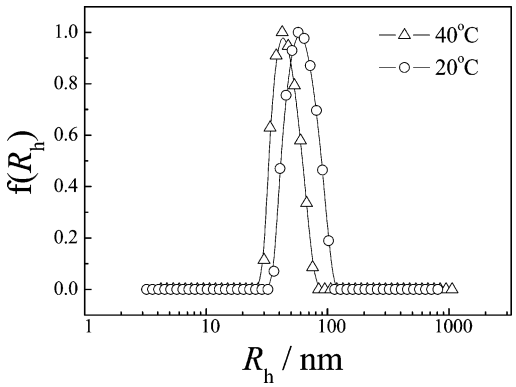

Figure 5. Temperature dependence of hydrodynamic radius distributions of hybrid nanoparticles prepared from $PNIPAM_{300}$-*b*-$PMPS_{52}$ by method 2. The concentration of nanoparticles is 5.0×10^{-6} g/mL.

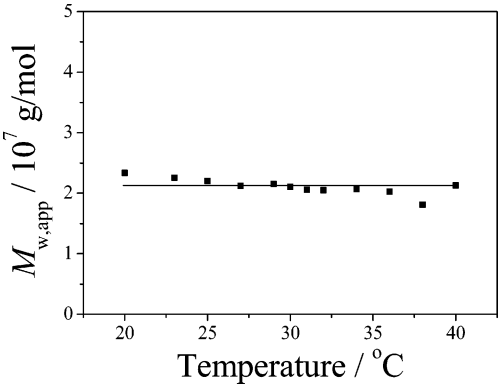

Figure 6. Temperature dependence of the apparent molecular weight, $M_{w,app}$, of hybrid nanoparticles prepared from $PNIPAM_{300}$-*b*-$PMPS_{52}$ by method 2. The concentration of nanoparticles is 5.0×10^{-6} g/mL.

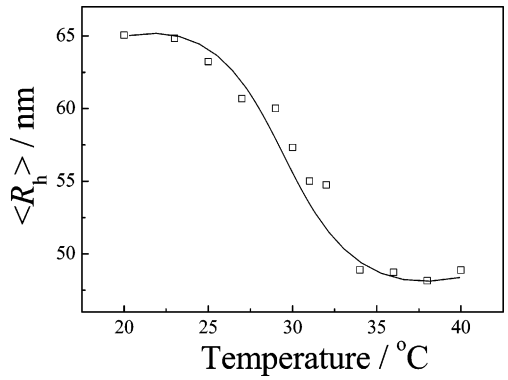

Figure 7. Temperature dependence of the average hydrodynamic radius, $\langle R_h \rangle$, of nanoparticles prepared from $PNIPAM_{300}$-*b*-$PMPS_{52}$ by method 2. The concentration of nanoparticles is 5.0×10^{-6} g/mL.

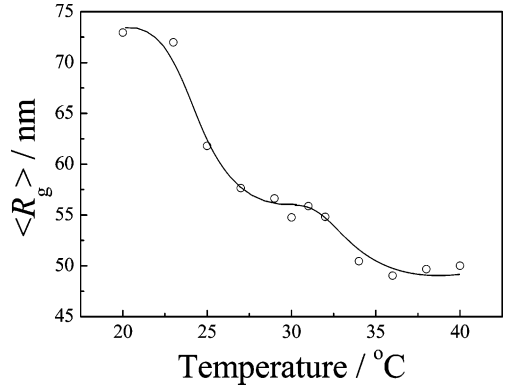

Figure 8. Temperature dependence of the average radius of gyration $\langle R_g \rangle$ of the nanoparticles prepared from $PNIPAM_{300}$-*b*-$PMPS_{52}$ by method 2. The concentration of nanoparticles is 5.0×10^{-6} g/mL.

aged molecular weight of $PNIPAM_{300}$-*b*-$PMPS_{52}$ is 46 900. After cross-linking, the weight-averaged molecular weight molecular weight of the block copolymer is calculated to be 50 600 g mol^{-1}, considering that the molecular weight distribution (M_w/M_n) determined by GPC is 1.17. The average aggregation number of block copolymer chains inside each hybrid nanoparticles is calculated to be 420. The TEM image shown in Figure 4b reveals an average silica core size of about 30 nm. So the grafting density of PNIPAM chains at the silica core surface can be calculated; the average surface area occupied per PNIPAM chain is ~6.7 nm^2. This reflects a relatively dense grafting of PNIPAM chains at the surface of silica core.

Figures 7 and 8 show the temperature dependence of the average hydrodynamic radius $\langle R_h \rangle$ and average radius of gyration $\langle R_g \rangle$ of the nanoparticles upon heating. Upon heating, $\langle R_h \rangle$ decrease monotonically from 65 to 48 nm in the temperature range 20−36 °C. This corresponds to a 60% decrease of the volume of prepared hybrid nanoparticles (Scheme 1). The diameter of the silica core is about 30 nm, so the thickness of PNIPAM brush at 20 °C is estimated to be 50 nm. The calculated end-to-end distance of fully extended PNIPAM chain with a DP of 300 is about 75 nm. In preliminary experiments, we found that $\langle R_h \rangle$ of free PNIPAM chains with a DP of 300 in water is ca. 7 nm; i.e., the dimensions of free PNIPAM chains are ~14 nm. This indicates that PNIPAM chains in the brush are partially extended due to steric exclusions exhibited by neighboring PNIPAM chains, but they are not fully extended.

The more fascinating thing is the temperature dependence of $\langle R_g \rangle$ (Figure 8). $\langle R_g \rangle$ is very sensitive to chain segment density distributions for polymer chains and core/shell nanoparticles. It clearly reveals that PNIPAM brush grafted on silica core undergo a two-stage collapse. The $\langle R_g \rangle$ is about 72 nm at 20 °C; it gradually decreases to 56 nm at 26 °C. A small plateau was reached in the range 26−30 °C. Above 31 °C, $\langle R_g \rangle$ further decreases from 55 to 49 nm in the temperature range 31−36 °C.

When PNIPAM chains are attached by one end to a flat substrate or curved interface (such as latex particles) with a sufficient density, referred to as a polymer brush, they are crowned and forced to stretch away from the solid surface to avoid overlapping. Theoretical predications suggest that the strong interchain interactions are present in the brush and cause a broadening of the transition of polymer chains.[55,56] Experimental results have already confirmed this predication. Zhu et al. have sterically or electrosterically stabilized PS latex particles with PNIPAM chains with DP of 3000 or 6000. In both cases, dynamic LLS reveals that the grafted PNIPAM layer exhibit a broad phase transition spanning ca. 20 °C, compared to ca. 1−2 °C for that of free PNIPAM chains.[57] Although the grafting density of PNIPAM chains at the latex surface was not reported in this system, it is not expected to be very high. So it is difficult to directly compare their results with ours. Tenhu et al. have grafted PNIPAM brush from gold nanoparticles; the DP of grafted PNIPAM chain is about 50, and the grafting density is very high, ca. 0.4 nm^2 per chain. Microcalorimetric measurements reveal two well-separated phase transitions for densely grafted PNIPAM brush at the gold core surface.

The results of the temperature dependence of $\langle R_g \rangle$ obtained here agrees quite well with observations made by Tenhu et al.; i.e., the PNIPAM brush exhibits a two-stage collapse. In our case, the grafting density of PNIPAM brush at the core surface is much lower, ca. 6.7 nm^2 per chain, and the DP of PNIPAM chain is 6 times larger, as compared to PNIPAM grafted gold nanoparticles reported by Tenhu et al.[9] The increase of chain length of grafted PNIPAM chain will render the brush more crowded due to the larger hydrodynamic volume occupied by each grafted chain; this will partially make up the decrease of chain crowding in the brush incurred by lower grafting density. We tentatively postulate that PNIPAM chain segments neighboring the silica core surface will undergo different chain crowding as compared to that at the outer part of PNIPAM brush. The inner part of the PNIPAM brush tends to collapse at lower temperatures due to the higher extent of chain crowding; this will more abruptly decrease $\langle R_g \rangle$ compared to $\langle R_h \rangle$. Thus, we observe double phase transitions of densely grafted PNIPAM brush at the silica core surface.

We also plotted the temperature dependence of the ratio $\langle R_g \rangle / \langle R_h \rangle$ which reflects the chain density distribution (Figure 8). The fact that at lower temperatures $\langle R_g \rangle / \langle R_h \rangle \sim 1.1$ can be attributed to the stretched conformation of PNIPAM brush due to chain crowding and interchain repulsion; this is also the typical $\langle R_g \rangle / \langle R_h \rangle$ value observed for hairy core−shell nanoparticles. $\langle R_g \rangle / \langle R_h \rangle$ decreased from 1.1 to 0.95 in the range 20−26 °C and then stabilized at around 0.95 in the range 26−30 °C. Above 30 °C, $\langle R_g \rangle / \langle R_h \rangle$ increases again to about 1.05 and stabilizes at that value above 36 °C. In comparison

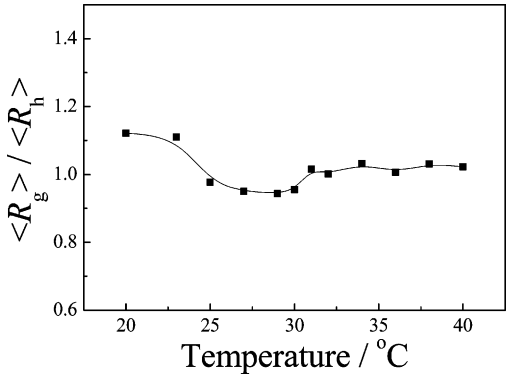

Figure 9. Temperature dependence of $\langle R_g \rangle / \langle R_h \rangle$ of the hybrid nanoparticles prepared from $PNIPAM_{300}$-*b*-MPS_{52} by method 2. The concentration of nanoparticles is 5.0×10^{-6} g/mL.

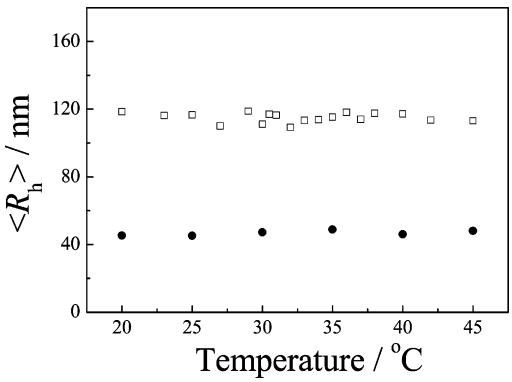

Figure 10. Temperature dependence of $\langle R_h \rangle$ of the hybrid nanoparticles prepared from $PNIPAM_{48}$-*b*-$PMPS_{60}$ by method 1 (□) and method 2 (○). The concentration of nanoparticles is 5.0×10^{-6} g/mL.

with a uniform sphere with the same size, the denser core leads to a smaller $\langle R_g \rangle$, but the same $\langle R_h \rangle$, so that $\langle R_g \rangle / \langle R_h \rangle$ is lowest in the temperature range where the inner part of PNIPAM brush start to collapse. Now it is quite clear that densely grafted PNIPAM brush on the silica surface undergoes a two-stage collapse. The first stage of collapse is due to the inner part of PNIPAM brush; this takes place in the temperature range 20−26 °C, while the outer part still remains solvated. Above 30 °C, the outer part of PNIPAM brush undergoes the second stage of collapse, which is accompanied by the increase in $\langle R_g \rangle / \langle R_h \rangle$ value.

It should be noted for $PNIPAM_{48}$-*b*-$PMPS_{60}$ the hybrid nanoparticles prepared by two different methods differ a lot in $\langle R_h \rangle$. Nanoparticles prepared by method 1 are much larger (110 nm) than that prepared by method 2 (50 nm). This is also in agreement with the TEM results. The $\langle R_h \rangle$ of nanoparticles prepared by two different approaches show no detectable temperature dependence, possibly due to the grafted PNIPAM brush being too shot (Figure 10). Combined with the results of Tenhu et al. and $PNIPAM_{300}$-*b*-$PMPS_{52}$ nanoparticles, we tentatively postulate that the double phase transition behavior of polymer brush at the silica core surface can be only observed when the grafting density is high enough and the polymer chain in the brush is long enough.

Turbidity Measurements. Figure 11 shows the temperature dependence of transmittance at 600 nm for nanoparticles prepared from $PNIPAM_{300}$-*b*-$PMPS_{52}$ by method 2. It should be noted that much higher concentration (8.0×10^{-4} g/mL) compared to that for light

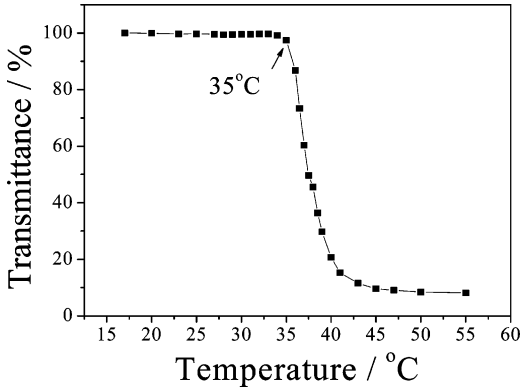

Figure 11. Temperature dependence of transmittance of an aqueous solution of hybrid nanoparticles prepared from $PNIPAM_{300}$-*b*-$PMPS_{52}$ by method 2. The concentration of nanoparticle is 8.0×10^{-4} g/mL.

scattering studies was used here to have enough detection sensitivity. Heating the nanoparticle solution at 5.0×10^{-6} g/mL (same concentration as used in light scattering) results in absolutely no change in transmittance from 15 to 55 °C. This is in agreement with the LLS results, where $M_{w,app}$ does not change with temperature (Figure 6). At a concentration of 8×10^{-4} g/mL, the transmittance exhibits no changes in the range 15−35 °C. It should be noted that LLS results reveal the complete collapse of PNIPAM brush below 35 °C. Above 35 °C, transmittance decreases abruptly from 100% to about 10−20% in the range 35−40 °C.

The decrease of transmittance should be correlated with the increase of scattering light intensity. So the transmittance decrease above 35 °C should be due to the aggregation of hybrid nanoparticles. Hybrid nanoparticles with already collapsed PNIPAM brush tend to collide with each other at the concentration studied; this kind of collision will surely contribute to the aggregation between different hybrid nanoparticles since the PNIPAM corona becomes "sticky" above their LCST. So the whole process associated with continuous heating of the hybrid nanoparticle at a concentration of 8×10^{-4} g/mL is as follows. The inner part of the PNIPAM brush collapses first in the range 20−26 °C; this is followed by the collapse of the outer part of the PNIPAM brush in the range 31−36 °C. Above 36 °C, aggregation between neighboring hybrid nanoparticles takes place.

One-Pot Synthesis. Since high conversion of MPS monomer can be achieved (>90%) using the PNIPAM macro-RAFT agent, the removal of residual MPS monomer can be easily achieved by in situ precipitation into hexane and decanting. Thanks to the RAFT technique used to prepare the PNIPAM-*b*-PMPS, there is no need to remove copper catalysts. After briefly drying the precipitated products under vacuum, DMF was added to dissolve the block copolymer to desired concentration; we then successfully prepared hybrid core−shell nanoparticles just in one-pot using either method 1 or method 2. These bodes well for the possibility of large-scale synthesis of this kind of novel thermoresponsive hybrid nanoparticle.

Conclusion

In aqueous solution, amphiphilic PNIPAM-*b*-PMPS self-assembles into micelles with PMPS core and PNIPAM shell. The base-catalyzed sol−gel process inside PMPS core results in PNIPAM encapsulated

silica hybrid core−shell nanoparticles. The monodisperse hybrid nanoparticles are densely grafted with PNIPAM brush at the surface of silica core. The PNIPAM brush exhibits two-stage thermoresponsive collapse upon heating through the LCST of the PNIPAM brush. We have also shown that one-pot synthesis of this kind of novel thermoresponsive hybrid core−shell nanoparticle is feasible. This is believed to be the first report of a stimuli-responsive hybrid core−shell nanoparticle via the block copolymer self-assembling approach.

Acknowledgment. This work is supported by an outstanding youth fund (50425310) from the National Natural Scientific Foundation of China (NNSFC) and the "Bai Ren" Project of the Chinese Academy of Sciences.

Note Added After ASAP Publication. This article was published ASAP on October 19, 2005. The author list published on this date was incorrect. The correct version was published on October 27, 2005.

References and Notes

(1) Alivisatos, A. P. *Science* **1996**, *271*, 933.
(2) Golden, J. H.; Deng, H. B.; Disalvo, F. J.; Thompson, P. M.; Frechet, J. M. *Science* **1995**, *268*, 1463.
(3) Ash, B. J.; Siegel, R. W.; Schadler, L. S. *Macromolecules* **2004**, *37*, 1358.
(4) Caruso, F. *Adv. Mater.* **2001**, *13*, 11.
(5) Astruc, D.; Daniel, M.-C. *Chem. Rev.* **2004**, *104*, 293.
(6) Bourgeat-Lami, E. In *Encyclopedia of Nanoscience and Nanotechnology*; Scientific Publishers: Los Angeles, 2004; Vol. 8, pp 305−332.
(7) Zhu, M.; Wang, L.; Exarhos, G. J.; Li, A. D. Q. *J. Am. Chem. Soc.* **2004**, *126*, 2656.
(8) Shan, J.; Nuopponen, M.; Jiang, H.; Kauppinen, E.; Tenhu, H. *Macromolecules* **2003**, *36*, 4526.
(9) Shan, J.; Chen, J.; Nuopponen, M.; Tenhu, H. *Langmuir* **2004**, *20*, 4671.
(10) Lindenblatt, G.; Schärtl, W.; Pakula, P.; Schmidt, M. *Macromolecules* **2000**, *33*, 9340.
(11) Kim, K. M.; Keum, D. K.; Chujo, Y. *Macromolecules* **2003**, *36*, 867.
(12) Ohno, K.; Morinaga, T.; Koh, K.; Tsujii, Y.; Fukuda, T. *Macromolecules* **2005**, *38*, 2137.
(13) Kim, J. H.; Lee, T. R. *Chem. Mater.* **2004**, *16*, 3647.
(14) Pyun, J.; Matyjaszewski, K.; Kowalewski, T.; Savin, D.; Patterson, G.; Kickelbick, G.; Huesing, N. *J. Am. Chem. Soc.* **2001**, *123*, 9455.
(15) von Werne, T.; Patten, T. E. *J. Am. Chem. Soc.* **1999**, *121*, 7409.
(16) Ohno, K.; Koh, K.; Tsujii, Y.; Fukuda, T. *Macromolecules* **2002**, *35*, 8989.
(17) Pyun, J.; Matyjaszewski, K. *Chem. Mater.* **2001**, *13*, 3436.
(18) Matsuno, R.; Yamamoto, K.; Otsuka, H.; Takahara, A. *Chem. Mater.* **2003**, *15*, 3.
(19) Mori, H.; Seng, D. C.; Zhang, M. F.; Müller, A. H. E. *Langmuir* **2002**, *18*, 3682.
(20) Chen, X.; Armes, S. P. *Adv. Mater.* **2003**, *15*, 1558.
(21) Perruchot, C.; Khan, M. A.; Kamitsi, A.; Armes, S. P.; von Werne, T.; Patten, T. E. *Langmuir* **2001**, *17*, 4479.
(22) Carrot, G.; Rutot-Houzé, D.; Pottier, A.; Degée, P.; Hilborn, J.; Dubois, P. *Macromolecules* **2002,** *35*, 8400.
(23) Bartholome, C.; Beyou, E.; Bourgeat-Lami, E.; Chaumont, P.; Zydowicz, N. *Macromolecules* **2003**, *36*, 7946.
(24) Hamley, I. W. In *The Physics of Block Copolymers*; Oxford University Press: Oxford, 1998; p 131.
(25) Zhang, L.; Eisenberg, A. *Science* **1995**, *268*, 1728.
(26) Zhang, L.; Eisenberg, A. *J. Am. Chem. Soc.* **1996**, *118*, 3168.
(27) Shen, H.; Eisenberg, A. *Macromolecules* **2000**, *33*, 2561.
(28) Ding, J.; Liu, G. *Macromolecules* **1997**, *30*, 655.
(29) Discher, B. M.; Won, Y.; Ege, D. S.; Lee, J. C.-M.; Bates, F. S.; Discher, D. E.; Hammer, D. A. *Science* **1999**, *284*, 1143.
(30) Jenekhe, S. A.; Chen, X. L. *Science* **1998**, *279*, 1903; *283*, 372.
(31) Li, Z. C.; Liang, Y. Z.; Li, F. M. *Chem. Commun.* **1999**, 1557.
(32) Sommerdijk, N. A. J. M.; Holder, S. J.; Hiorns, R. C.; Jones, R. G.; Nolte, R. J. M. *Macromolecules* **2000**, *33*, 8289.
(33) van Hest, J. C. M.; DeInoye, D. A. P.; Baars, M. W. P. L.; van Genderen, M. H. P.; Meijer, E. W. *Science* **1995**, *268*, 1592.
(34) Vriezema, D. M.; Hoogboom, J.; Velonia, K.; Takazawa, K.; Christianen, P. C. M.; Maan, J. C.; Rowan, A. E.; Nolte, R. J. M. *Angew. Chem., Int. Ed.* **2003**, *42*, 772.
(35) (a) Thurmond, K. B.; Kowalewski, T.; Wooley, K. L. *J. Am. Chem. Soc.* **1996**, *118*, 7239. (b) Thurmond, K. B.; Kowalewski, T.; Wooley, K. L. *J. Am. Chem. Soc.* **1997**, *119*, 6656. (c) Wooley, K. L. *J. Polym. Sci., Part A: Polym. Chem.* **2000**, *38*, 1397.
(36) Maskos, M.; Harris, J. R. *Macromol. Rapid Commun.* **2001**, *22*, 271.
(37) (a) Wang, X. S.; Arsenault, A.; Ozin, G. A.; Winnik, M. A.; Manners, I. *J. Am. Chem. Soc.* **2003**, *125*, 12686. (b) Underhill, R. S.; Liu, G. *Chem. Mater.* **2000**, *12*, 2082. (c) Stewart, S.; Liu, G. *Chem. Mater.* **1999**, *11*, 1048.
(38) (a) Hui, T.; Chen, D.; Jiang, M. *Macromolecules* **2005**, *38*, 5834. (b) Chen, D.; Jiang, M. *Acc. Chem. Res.* **2005**, *38*, 494. (c) Peng, H.; Chen, D.; Jiang, M. *Macromolecules* **2005**, *38*, 3550.
(39) Hadjichristidis, N.; Iatrou, H.; Pitsikalis, M.; Pispas, S.; Avgeropoulos, A. *Prog. Polym. Sci.* **2005**, *30*, 725.
(40) Rodríguez-Hernández, J.; Chécot, F.; Gnanou, Y.; Lecommandoux, S. *Prog. Polym. Sci.* **2005**, *30*, 691.
(41) Bütün, V.; Billingham, N. C.; Armes, S. P. *J. Am. Chem. Soc.* **1998**, *120*, 11818.
(42) Liu, S.; Weaver, J. V. M.; Save, M.; Armes, S. P. *Langmuir* **2002**, *18*, 8350.
(43) Du, J.; Chen, Y.; Zhang, Y.; Han, C. C.; Fischer, K.; Schmidt, M. *J. Am. Chem. Soc.* **2003**, *125*, 14710.
(44) (a) Du, J.; Chen, Y. *Macromolecules* **2004**, *37*, 6322. (b) Du, J.; Chen, Y. *Macromolecules* **2004**, *37*, 5710.
(45) (a) Du, J.; Chen, Y. *Angew. Chem., Int. Ed.* **2004**, *43*, 5084. (b) Du, J.; Chen, Y. *Macromol. Rapid Commun.* **2005**, *26*, 491.
(46) Du, J.; Armes, S. P. *J. Am. Chem. Soc.* **2005**, *127*, 12800.
(47) Chiefari, J.; Chong, Y. K.; Ercole, F.; Krstina, J.; Le, T. P. T.; Mayadunne, R. T. A.; Meijs, G. F.; Moad, G.; Moad, C. L.; Rizzardo, E.; Thang, S. H. *Macromolecules* **1998**, *31*, 5559.
(48) (a) Thang, S. H.; Chong, Y. K.; Mayadunne, R. T. A.; Moad, G.; Rizzardo, E. *Tetrahedron Lett.* **1999**, *40*, 2435. (b) Le, T. P.; Moad, G.; Rizzardo, E.; Thang, S. H. WO Patent No. 9801478, 1998.
(49) Rizzardo, E.; Chiefari, J.; Mayadunne, R. T. A.; Moad, G.; Thang, S. H. *ACS Symp. Ser.* **2000**, *768*, 278.
(50) Mellon, V.; Rinaldi, D.; Bourgeat-Lami, E.; D'Agosto, F. *Macromolecules* **2005**, *38*, 1591.
(51) Li, C.; Benicewicz, B. C. *Macromolecules* **2005**, *38*, 5929.
(52) Schilli, C.; Lanzendorfer, M. G.; Muller, A. H. E. *Macromolecules* **2002**, *35*, 6819.
(53) Cameron, N. S.; Corbierre, M. K.; Eisenberg, A. *Can. J. Chem.* **1999**, *77*, 1311.
(54) Schild, H. G. *Prog. Polym. Sci.* **1992**, *17*, 163.
(55) Zhao, B.; Brittain, W. J. *Prog. Polym. Sci.* **2000**, *25*, 677.
(56) Halperin, A.; Tirrell, M.; Lodge, T. P. *Adv. Polym. Sci.* **1992**, *100*, 31.
(57) Zhu, P. W.; Napper, D. H. *J. Colloid Interface Sci.* **1994**, *164*, 489.

MA0518050